PHYSICAL REVIEW B VOLUME 32, NUMBER 12 15 DECEMBER 1985

Raman study of phonon anharmonicity in LaF_3

E. Liarokapis, E. Anastassakis, and G. A. Kourouklis
Physics Laboratory III, National Technical University, 157 73 Athens, Greece
(Received 29 July 1985)

The first-order Raman spectrum of LaF_3 was studied as a function of hydrostatic pressure (0—10 GPa) and temperature (60—900 K). The calculated values for the mode Grüneisen parameters are between 1 and 2, in reasonable agreement with those derived from uniaxial-stress experiments. Deviations from the isotropic approximation, in handling the temperature dependence of the long-wavelength optical-phonon frequencies, are found to be smaller than 15%. Anharmonicity contributions to the phonon frequencies and half-widths are calculated from the joint data. The results indicate that for most of the phonons it is the volume contributions that are mainly responsible for the temperature-induced frequency shifts. Anharmonicity appears to be important for fewer phonons and also for the increase of linewidth with temperature for all phonons studied. Other observations are also discussed, such as the pressure dependence of the phonon linewidths and the frequency dependence of the frequency-versus-pressure slopes.

I. INTRODUCTION

Lanthanum trifluoride, LaF_3, is a wide-band-gap insulator known for its interesting variations of lattice structure and electronic properties and for its potential use as a laser host material.[1,2] The long-standing controversy about its structure being D_{6h}^3 ($P6_3/mcm$) or D_{3d}^4 ($P\bar{3}c1$) seems to have been resolved, in favor of the latter, according to the original Raman work of Bauman and Porto,[3] and the most recent Raman stress measurements of Cerdeira *et al.*[4] Information about its thermal,[5–7] elastic,[8] and optical[9] properties are rather limited, but nevertheless sufficient to allow an anharmonicity study to be undertaken, based on our Raman measurements under variable temperatures (T) and hydrostatic pressures (P). From such experiments we have obtained values of the mode Grüneisen parameters for the Raman-active long-wavelength optical phonons ω_j (called phonons, for simplicity, from now on). In fact, we have established the exact (linear) T dependence of the mode Grüneisen parameters by combining (a) existing information from the literature about the T dependence of the thermal expansion coefficient and of the volume compressibility and (b) our observation that the slopes $(\partial\omega_j/\partial P)_T$ are independent of T.

The above information, together with our measurements of the T-dependent phonon frequencies $\omega_j(T)$, lead to an estimate of the various contributions to the T-dependent frequency shifts $\Delta\omega_j$ and phonon damping constants $\Gamma_j(T)$. The present calculations show that for most of the phonons the volume contribution to $\Delta\omega_j$ is substantial. This result is consistent with the overall ionic character of the material. Furthermore, it has become possible to asses the validity of the isotropic approximation.[10] The latter consists in ignoring the T dependence of the ratio of the two lattice constants a_1 to a_3. We find that deviations from the isotropic approximation do not exceed 15%, and, therefore, such approximation is well justified for all phonons studied. Finally, the slopes $(\partial\omega_j/\partial P)_T$ were found to depend on ω_j, in a linear fashion, while the phonon linewidths Γ_j show a definite tendency to increase with P.

The organization of the paper is as follows. In Sec. II we present the experimental details and results for both the T and P measurements. Section III deals with the T dependence of volume compressibility and thermal expansion coefficient and also with the so-called phonon deformation potentials. In Sec. IV the Grüneisen coefficients are calculated while the various contributions to the frequency shifts are analyzed in Sec. V. The validity of the isotropic approximation is checked in Sec. VI. The three- and four-phonon anharmonic terms are analyzed in Sec. VII, and Sec. VIII completes this work with remarks and conclusion.

II. EXPERIMENTAL PROCEDURE AND RESULTS

The Raman spectra were taken with a Spex double monochromator operating with holographically ruled gratings, an RCA-31034 cooled photomultiplier, and a phonon counting detection system. The various lines of an Ar^+ and Kr^+ laser were used as excitation radiation.

A. Temperature measurements

The samples were of parallelepiped shape with dimensions $\sim 3\times 2\times 2$ mm^3. Their long axes were along either z (optic axis) or y. The remaining two axes were along either the two-fold axes (x,y) of the D_{3d} point group or the axes (x,z), respectively.

The low-temperature measurements (typical accuracy ± 2 K) were taken with the sample inside a closed-cycle Dewar (Cryogenics Technology). For the high-temperature measurements the sample was mechanically attached on a ceramic finger which was electrically heated inside an evacuated high-temperature cell. The sample position could be chosen so as to allow application of the selection rules. The latter were necessary for observing

the phonons of various symmetries. In most of the cases a 90° scattering geometry was followed. A chromel-alumel thermocouple (with one of its contacts attached to the sample) was used to measure the high temperature, with accuracy and stability of ±2 K.

Typical T-dependent Raman spectra are shown in Fig. 1, while in Figs. 2 and 3 we present the peak frequencies ω_j and half-widths Γ_j as a function of T, for the various phonons studied. The solid curves in Fig. 2 have been drawn to assist the eye. The frequencies are designated by the corresponding values $\omega_j(0)$ which are obtained in Sec. VII.

The frequencies of the phonons in Fig. 2 were derived from smoothed data stored in a LeCroy 3500 MCA. The same applies for the half-widths (full widths at half maxima) which, before being included in Fig. 3, were first corrected for the instrumental broadening ($\sim$2.8 cm^{-1}) following standard techniques.[11] The average values of the frequencies observed at 60 and 90 K are listed in Table I under 75 K together with the results of Refs. 3 and 4 for comparison. We have observed two phonons of symmetry A_{1g} (out of five expected) and nine phonons of symmetry E_g (out of 12 expected) following the notation of the D_{3d} point group.[4]

The frequencies in Table I differ by at most 3 cm^{-1}. Such deviations in the results of these three sources may be attributed to a variety of experimental reasons. Since we are mainly interested in frequency shifts, we tend to ignore such differences in the absolute values of the phonon frequencies.

Not all phonons listed in Table I were studied at higher temperatures. The main reasons for this were the low scattering intensity of some modes and the interfering of adjacent modes because of their increasing linewidth at higher temperatures. The modes studied practically coincide with those investigated under uniaxial stress in Ref. 4, and under hydrostatic pressure (see the following section). This provides all of the necessary complementary data for testing the results and handling the thermodynamical aspects of the problem more thoroughly.

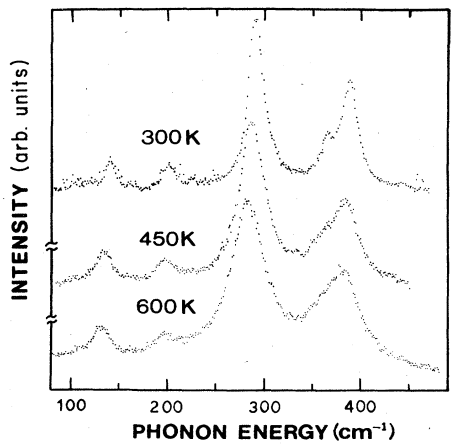

FIG. 1. Typical spectra of LaF_3 at three temperatures. Laser wavelength and power are 514.5 nm and 400 mW. Scattering geometry is $x(yy)\bar{x}$.

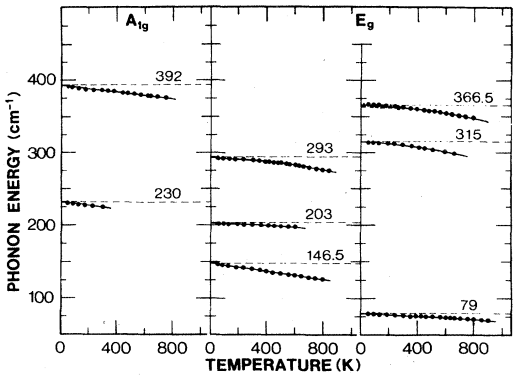

FIG. 2. Observed frequencies as a function of T. The solid lines are a guide to the eye. The dashed lines indicate the $\omega(0)$ values (in cm^{-1}) obtained in Sec. VII. Triangles (366.5 cm^{-1}) are data from Ref. 29.

B. Hydrostatic pressure measurements

The hydrostatic pressure measurements were taken with a diamond anvil cell.[12] Otherwise, the same experimental arrangement was used as the one described at the beginning of this section. The 25 K measurements were taken at the Max-Planck Institut for Solid State Physics, Stuttgart. Independent measurements at 300 K were performed in Athens and the results were consistent with those at 25 K as will be discussed below. Instrumental linewidths were 3.5 cm^{-1} and 2.8 cm^{-1}, respectively.

The sample and the ruby chip used for calibration floated in a 4:1 methanol-ethanol mixture for room temperature measurements, while at 25 K the surrounding medium was solid argon.[12] For an observed frequency shift $\Delta\omega$ (in cm^{-1}) of the $R_{1,2}$ fluorescence lines of ruby, the corresponding pressure (in GPa) was $0.132\Delta\omega$, at 25 and 300 K.[13]

Typical spectra for various pressures are shown in Fig. 4 at 300 K, while Fig. 5 shows collectively the P-dependent frequencies ω_j for those phonons of Table I which were studied under pressure at temperatures of 25 and 300 K. The phonon shifts are well represented by straight lines (least-square fits). Their slopes at $T=25$

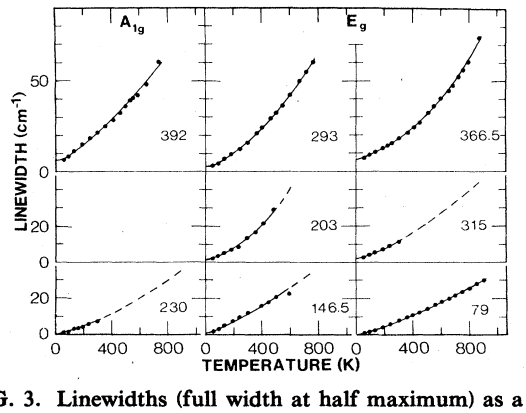

FIG. 3. Linewidths (full width at half maximum) as a function of T. Instrumental corrections have been included. The solid line represents best fit of Eq. (22). Frequency values are in cm^{-1} as in Fig. 2.

TABLE I. Phonon frequencies of LaF_3, their deformation potentials and pressure derivatives, and Grüneisen parameters for the same phonons.

Symmetry D^4_{3d}	ω(cm^{-1}) 70 K[a]	77 K[b]	75 K[c]	$(\partial\omega/\partial P)_T$ (cm^{-1}/GPa) 25 K	300 K	Phonon deformation potentials (cm^{-1}/GPa) a'	b'	a (cm^{-1})	b	γ^T 77 K c	d
A_{1g}	231	228.5	229.8	2.4±0.2	2.0±0.1	0.7±0.1	−1.1±0.5	122.7	−161.6	1.19±0.15	0.15±0.26
	390	389.5	391.0	5.6±0.1	5.7±0.1	1.3±0.2	5.1±0.8	649	1286	1.64±0.11	2.19±0.25
E_g	145	144.6	146.2	1.5±0.2	1.8±0.1	1.6±0.1	−1.1±0.5	364	−55	1.17±0.21	1.65±0.42
	203	202.0	202.5	3.1±0.1	2.8±0.3	0.2±0.1	1.1±0.6	119	268	1.75±0.15	0.83±0.35
	290	292.7	293.0	3.9±0.1	4.1±0.1	1.2±0.1	0.3±0.6	339	208	1.52±0.11	1.02±0.24
		299.4	299.8	4.5±0.2		3.2±0.2	−1.0±0.9	799	156	1.64±0.15	1.99±0.36
	79	77.6	78.6		0.83±0.04	0.5±0.1	−0.5±0.5	105	−52	1.02±0.10	0.71±0.77
	163	163.1	163.2								
	315	314.0	315.1	5.5±0.1	6.4±0.5	4.2±0.2	−2.1±0.6	1002	29	2.0±0.14	2.24±0.26
	366	365.0	366.0[e]	4.9±0.1	5.0±0.1					1.52±0.11	

[a]See Ref. 3.
[b]See Ref. 4.
[c]From the present paper.
[d]Based on Eq. (12c) and the data of Ref. 4.
[e]At lower temperatures this line splits into a doublet, at 365.6 and 368.4 cm^{-1}.

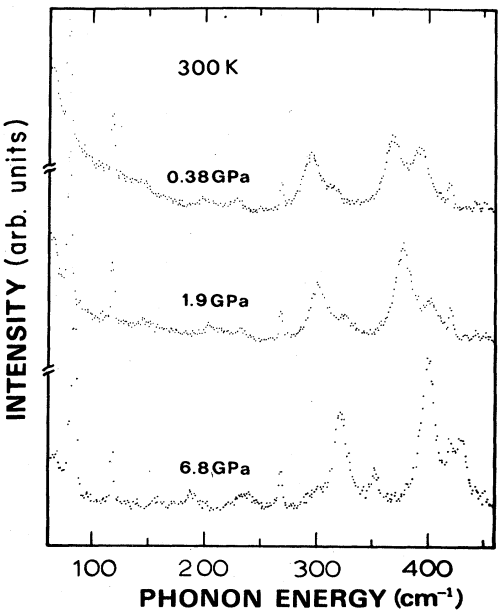

FIG. 4. Typical spectra of LaF_3 at 300 K for three different pressures. Wavelength is $\lambda = 514.5$ nm and power is 200 mW.

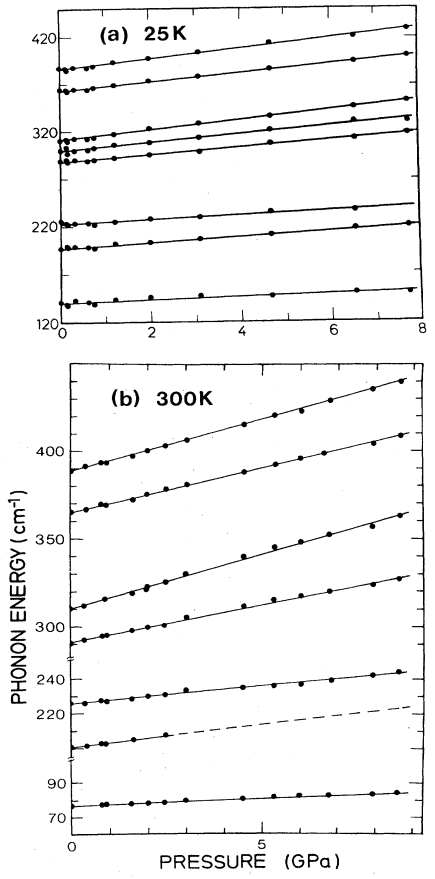

FIG. 5. Observed frequencies as a function of P at (a) 25 K and (b) 300 K. Solid lines are the results of (linear) best fit.

and 300 K are listed in Table I and will be used in the following section for the calculation of the mode Grüneisen parameters. Quadratic terms in P appear to exist for both temperatures but were ignored as unimportant for the purpose of the present analysis, which is valid in the limit of $P\rightarrow 0$. Since, as yet, no experimental or analytic information seems to exist about Murnaghan's equation of state,[14] we defer from plotting ω_j in terms of the percentage changes $\Delta a_1/a_1$ and $\Delta a_3/a_3$ of the two lattice constants.

The most interesting fact is that for all phonons studied, the pressure slopes at 25 and 300 K appear to be equal, within experimental error. Accordingly, such slopes will be treated as T independent in the subsequent analysis and set equal to their values at 25 K, as more accurate.

III. ELASTIC AND THERMAL PROPERTIES

Elastic constants, thermal expansion coefficients, phonon deformation potentials, and Grüneisen parameters are the main crystal properties that will be used in the following sections for the analysis of the present data. Some of this information is taken from the literature, the rest is derived here.

A. Elastic constants

The elastic stiffnesses C_{ij} of LaF_3 and their T dependence in the range from under 100 to about 600 K have been measured by Laiho *et al.*[8] In terms of C_{ij} the elastic compliances are[15]

$$S_{11}=\frac{1}{2}\left[\frac{C_{33}}{C}+\frac{1}{C_{11}-C_{12}}\right], \tag{1a}$$

$$S_{12}=\frac{1}{2}\left[\frac{C_{33}}{C}-\frac{1}{C_{11}-C_{12}}\right], \tag{1b}$$

$$S_{13}=-\frac{C_{13}}{C}, \tag{1c}$$

$$S_{33}=\frac{C_{11}+C_{12}}{C}, \tag{1d}$$

$$S_{44}=\frac{1}{C_{44}}, \tag{1e}$$

$$S_{66}=2(S_{11}-S_{12})=\frac{2}{C_{11}-C_{12}}, \tag{1f}$$

where

$$C=C_{33}(C_{11}+C_{12})-2C_{13}^2 . \tag{1g}$$

The above expressions correspond to the hexagonal point group D_{6h} which differs from D_{3d} only with regard to the presence in the latter of an additional component C_{14}. As shown in Ref. 8, this component is nearly zero in LaF_3 which means that S_{14} is nearly zero too. Under these circumstances Eqs. (1) are valid for D_{3d} as well.

Finally, the linear and bulk compressibilities are[15]

$$\kappa_1=S_{11}+S_{12}+S_{13}, \tag{2a}$$

$$\kappa_3=2S_{13}+S_{33}, \tag{2b}$$

and

$$\kappa=2\kappa_1+\kappa_3 . \tag{3}$$

Using the T-dependent values of C_{ij} we have found that as a function of T, the bulk compressibility is very well described by the analytical form

$$\kappa(T)=A+BT+\frac{C}{T+D}, \tag{4}$$

where

$$A=0.81/\text{GPa},\quad B=0.25\times 10^{-5}/(\text{GPa K}),$$

$$C=12.6\ \text{K/GPa},\quad D=225\ \text{K}.$$

This expression is shown in Fig. 6 together with the data and will be used shortly in deriving the T dependence of the mode Grüneisen parameters. It is noted that by construction the slope of the above function becomes zero as $T\rightarrow 0$. This is imposed by the validity of similar conditions for the stiffnesses C_{ij}.[8]

B. Thermal expansion coefficients

The only data relevant to thermal expansion which are available from the literature are those in Ref. 5. They concern measurements of the percentage expansion of bulk crystal dimensions as a function of temperature (above room temperature) along two directions, parallel and perpendicular to the optic axis. From these data we calculate values for the integrals

$$I_1(T)=\int_0^T \beta_1(T')dT'+c_1, \tag{5a}$$

$$I_3(T)=\int_0^T \beta_3(T')dT'+c_2, \tag{5b}$$

where β_1,β_3 are the linear thermal expansion coefficients and c_1,c_2 are arbitrary constants. From Eqs. (5) then we have

$$I(T)=2I_1(T)+I_3(T)=\int_0^T \beta(T')dT'+c, \tag{6}$$

where β is the volume thermal expansion coefficient. The function $I(T)$ is plotted in Fig. 7 within an arbitrary constant. Differentiating Eq. (6) gives directly the function $\beta(T)$. Selective points of the latter are shown in Fig. 7 in the region above 300 K. For $T<300$ K we performed an independent calculation of $\beta(T)$. It was based on existing data for the Debye temperatures[8] and the expression[16]

$$\beta(T)=\beta_\infty D(\Theta_D/T), \tag{7}$$

where $D(\eta)$ is the Debye integral given by[17]

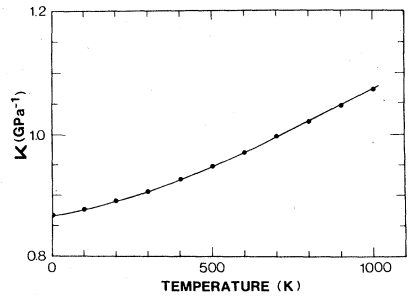

FIG. 6. Temperature dependence of volume compressibility κ. The solid line represents best fit [Eq. (4)] to experimental points of Ref. 8 combined with Eqs. (1)—(3).

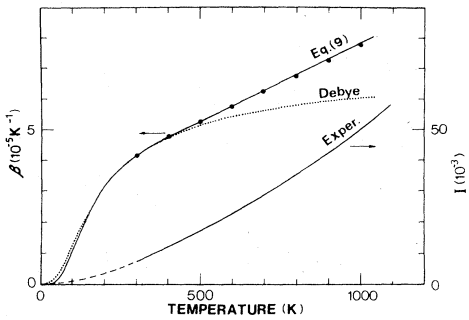

FIG. 7. Temperature dependence of the integral $I(T)$ of Eq. (6) and its derivative $\beta(T)$ (volume expansion coefficient and data points). The dotted line represents the Debye model of $\beta(T)$ normalized to the data at $T=300$ K (Ref. 8). The solid line (left-hand scale) represents values of $\beta(T)$ according to Eq. (9).

$$D(\eta)=\frac{3}{\eta^3}\int_0^{\eta}\frac{\xi^4}{(e^{\xi}-1)^2}d\xi\ . \tag{8}$$

The multiplication factor β_∞ represents a limiting value of β at high temperatures and is chosen here so that Eq. (7) will produce the correct value for β at 300 K.

The results of Eq. (7) are shown by the dotted line in Fig. 7. The curve and the data points are in good agreement in the temperature region between 300 and 500 K, while for higher temperatures they differ by no more than 25%. It should be noted, however, that such differences would not affect significantly the results of the calculations in the following sections. In any case, we have chosen to keep the experimental data points above 300 K and the values of Eq. (7) (dotted curve) below 300 K. It was found that the entire region (0—1000 K) is very well covered by the analytical form

$$\beta(T)=\left[\frac{A}{T}+\frac{B}{T^2}\right]\sinh^{-2}(T_1/T)\ , \tag{9}$$

where $A=1.7\times10^{-3}$, $B=1.4$ K, and $T_1=200$ K (shown by the solid line in Fig. 7). Such an expression fulfills the basic requirement that $\beta\to0$ as $T\to0$. The factor $\sinh^{-2}(T_1/T)$, in particular, has been shown to enter the expressions for β reached through detailed lattice-dynamical calculations.[18]

C. Phonon deformation potentials

An important set of phenomenological parameters for the calculations in the following section are the *phonon deformation potentials.* They are defined from the slopes of phonon frequency shifts as a function of the various applied stress components σ_{ij}. There are altogether four such coefficients for this particular crystal structure (D_{3d}). Their values for those phonons of LaF_3 which were studied under uniaxial stress can be found in Ref. 4 as a',b',c',d' in cm^{-1}/kbar. An alternative set of such potentials is a,b,c,d in cm^{-1}, and this set relates phonon frequency shifts with the strain components ϵ_{ij}. The two sets are connected by

$$a'=a(S_{11}+S_{12})+bS_{13}\ , \tag{10a}$$

$$b'=2aS_{13}+bS_{33}\ , \tag{10b}$$

$$c'=c(S_{11}-S_{12})+\tfrac{1}{2}S_{14}d\ , \tag{10c}$$

$$d'=2cS_{14}+\tfrac{1}{2}S_{44}d\ , \tag{10d}$$

from which one finds

$$a=(a'S_{33}-b'S_{13})/S'\ , \tag{11a}$$

$$b=[-2a'S_{13}+b'(S_{11}+S_{12})]/S'\ , \tag{11b}$$

$$c=(c'S_{44}-d'S_{14})/S''\ , \tag{11c}$$

$$d=[-4c'S_{14}+2d'(S_{11}-S_{12})]/S''\ , \tag{11d}$$

where

$$S'=S_{33}(S_{11}+S_{12})-2S_{13}^2\ , \tag{11e}$$

$$S''=S_{44}(S_{11}-S_{12})-2S_{14}^2\ , \tag{11f}$$

and

$$S_{14}\simeq0\ .$$

Only the values of a',b' (or a,b) will be needed here, and for this reason we include them in Table I. They correspond to 77 K, and although no information exists about their temperature dependence, we can at least assume that the sum $2a'+b'$ is temperature independent, judging from the fact that $(\partial\omega/\partial P)_T$ is found to be insensitive to temperature (Table I).

IV. GRÜNEISEN PARAMETERS

The isothermal mode Grüneisen parameters γ_j^T can be calculated directly from the slopes of Fig. 5 and, alternatively, from the phonon deformation potentials. For the rest of this work, we omit the index j from all phonon-related quantities. We have then

$$\gamma^T=-\left[\frac{\partial\ln\omega}{\partial\ln V}\right]_T \tag{12a}$$

$$=\frac{1}{\kappa\omega}\left[\frac{\partial\omega}{\partial P}\right]_T \tag{12b}$$

$$=\frac{1}{\kappa\omega}(2a'+b') \tag{12c}$$

$$=\frac{2a\kappa_1+b\kappa_3}{\kappa\omega}\ , \tag{12d}$$

where the compressibilities from Eqs. (2) and (3) are used. It is emphasized that while Eq. (12a) stands for a general definition of γ^T, Eqs. (12b)—(12d) directly related γ^T to either the experimental slopes of Fig. 5 or the deformation potentials a',b' (or a,b). The latter are obtained from a totally different experimental procedure, namely, Raman measurements in the presence of uniaxial stresses. Thus, a direct comparison is possible between the values of γ^T obtained from the data of both experiments.

The results for γ^T at 77 K based on Eq. (12c) are listed in Table I. Next, we estimate the values of γ^T at 77 K,

based on Eq. (12b). for this reason we use the measured slopes $(\partial\omega/\partial P)_T$ at 25 K which we regard independent of temperature, according to the discussion at the end of Sec. II, and also the values of $\omega(T)$ and $\kappa(T)$ at 77 K from Fig. 2, and Fig. 6 or Eq. (4), respectively. The results are also shown in Table I. The error figures are based on the errors of a', b' (Ref. 4) and on our estimated errors on the slopes and the bulk modulus. Considering all experimental errors, in most of the cases the results are in general agreement. There is no obvious explanation for the significant difference found for two phonons (202.5 and 229.8 cm^{-1}). Since repeating our pressure measurements for these two phonons did not alter the numbers significantly, we feel that repetition of the far more sensitive stress measurements may produce additional information in this regard.

To complete the study of Grüneisen parameters, we calculated their values for the entire temperature range from 0 to 900 K, using the T-independent slopes at 25 K and the appropriate values for $\omega(T)$ and $\kappa(T)$. The results are shown in Fig. 8. The changes of $\gamma^T(T)$ in the above range are linear and vary between 0% and 13%. this is not a negligible variation and, under the condition of T-independent slopes $(\partial\omega/\partial P)_T$, represents the net effect of the competing functions $\omega(T)$ and $\kappa(T)$ shown in Figs. 2 and 6. Even if one allows some systematic change with T of the slopes $(\partial\omega/\partial P)_T$, the functions $\gamma^T(T)$ may be different in general, but it is very improbable that they will remain constant. We conclude this section by recognizing that, contrary to published cases[16,19–21], the mode Grüneisen parameters exhibit a measurable temperature dependence in general.

V. CONTRIBUTION TO THE FREQUENCY SHIFT

The phonon frequency shift caused by a change in temperature under constant pressure consists of two contributions according to the general thermodynamical expression[21,22]

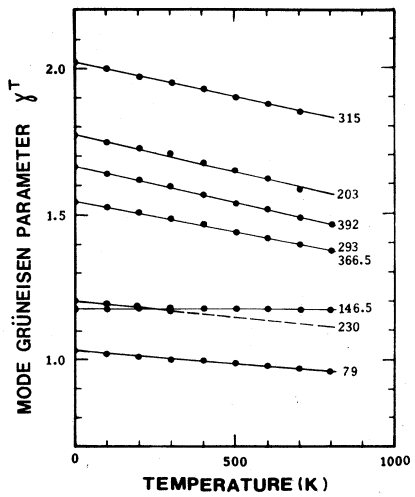

FIG. 8. Calculated dependence of mode Grüneisen parameters γ^T on T. The function $\kappa(T)$ of Eq. (4) and the T-dependent phonon frequencies from Fig. 2 were used.

$$\left[\frac{\partial\omega}{\partial T}\right]_P=-\frac{\beta}{\kappa}\left[\frac{\partial\omega}{\partial P}\right]_T+\left[\frac{\partial\omega}{\partial T}\right]_V=-\beta\omega\gamma^T+\left[\frac{\partial\omega}{\partial T}\right]_V . \tag{13}$$

Strictly speaking, Eq. (13) is valid for cubic materials only but can be and has been used for noncubic materials, assuming that the isotropic approximation is valid.

The two terms in the right-hand side of Eq. (13) stand for the *implicit* (volume-driven) effect and the *explicit* (occupation number-driven or amplitude-driven) effect.[22] An alternative form for Eq. (13) is the following:

$$\gamma^P(T)=\gamma^T(T)+\gamma^V(T) , \tag{14}$$

where by analogy to Eq. (12b) we have defined T-dependent Grüneisen parameters under constant pressure and under constant volume, i.e.,

$$\gamma^P(T)=-\frac{1}{\beta}\left[\frac{\partial\ln\omega}{\partial T}\right]_P , \tag{15a}$$

$$\gamma^V(T)=-\frac{1}{\beta}\left[\frac{\partial\ln\omega}{\partial T}\right]_V=-\frac{1}{\kappa}\left[\frac{\partial\ln\omega}{\partial P}\right]_V . \tag{15b}$$

According to its definition $\gamma^P(T)$ can be obtained from the slopes of Fig. 2 in the same way that $\gamma^T(T)$ is obtained from the slopes of Fig. 5. Clearly, the mode Grüneisen parameter γ^T is equal to γ^P only if the quasiharmonic approximation is valid. In that case, $\gamma^V=0$ and, therefore, $\gamma^P=\gamma^T$. In the most general case, $\gamma^V(T)$ is not zero. Its value can be estimated from the difference $\gamma^P(T)-\gamma^T(T)$ and represents a measure for the anharmonic contributions to the frequency shifts (explicit effect).

In Table II the values of γ's for various phonons are listed at 300 K, together with the corresponding terms of Eq. (13) for comparison. The *implicit fraction* η in Table II represents the ratio of the implicit to the total term (third to second or sixth to fifth column). This will be discussed in Sec. VIII.

In terms of finite differences, Eq. (13) provides a more convenient way for describing the anharmonic contributions. Upon integrating Eq. (13) from an appropriately chosen low-temperature T_0 to T, one obtains

$$\Delta\omega_{\text{total}}(T)=\Delta\omega_{\text{vol}}(T)+\Delta\omega_{\text{expl}}(T) , \tag{16}$$

where, from Fig. 2 and for $P=1$ bar,

$$\Delta\omega_{\text{total}}(T)=\omega(T)-\omega(0) , \tag{17}$$

that is, the curves of Fig. 2 give directly $\Delta\omega_{\text{total}}(T)$. Similarly,

$$\Delta\omega_{\text{vol}}(T)=-\int_{T_0}^{T}\frac{\beta}{\kappa}\left[\frac{\partial\omega}{\partial P}\right]_T dT' \tag{18a}$$

$$=-\int_{T_0}^{T}\beta\omega\gamma^T dT' \tag{18b}$$

$$\simeq-\omega(0)\gamma^T\int_{T_0}^{T}\beta dT' . \tag{18c}$$

Obviously Eq. (18c) is valid only under the assumption

TABLE II. Implicit (third or sixth column in the isotropic, and ninth column in the anisotropic approximation), and explicit (fourth or seventh column) contributions to the total effect (second or fifth column), implicit fraction η (eighth column), and difference of isotropic and anisotropic implicit contribution (absolute in tenth column, percentage in eleventh column). All entries correspond to 300 K.

Symmetry				$\left[\frac{\partial\omega}{\partial T}\right]_P=-\beta\omega\gamma^T+\left[\frac{\partial\omega}{\partial T}\right]_V$				$2\beta_1 a+\beta_3 b$		
D_{3d}^4	$\gamma^P=\gamma^T+\gamma^V$			(10^{-3})			η	(10^{-3})	$\lvert\alpha\rvert$	$\lvert\alpha/\beta\omega\gamma^T\rvert$	%
$A_{1g}(230)$	1.70	1.17	0.53	−15.8±1.4	−10.9	−4.9±1.7	0.69±0.13	0.32	0.69		6.3
$A_{1g}(392)$	1.42	1.60	−0.18	−22.5±1.5	−25.4	2.9±1.6	1.13±0.08	48.80	1.54		6.1
$E_g(146.5)$	4.75	1.18	3.57	−27.4±0.6	−6.8	−20.6±1.2	0.25±0.04	10.29	1.02		15.0
$E_g(203)$	1.22	1.71	−0.49	−10.0±0.7	−14.1	4.1±0.9	1.40±0.11	9.66	0.36		2.6
$E_g(293)$	1.97	1.48	0.49	−23.5±0.9	−17.6	−5.9±1.0	0.75±0.04	15.29	0.32		1.8
$E_g(299)$		1.64			−20.1			28.68	1.56		7.8
$E_g(79)$	3.41	1.00	2.41	−10.8±0.3	−3.2	−7.6±0.3	0.29±0.01	2.17	0.38		11.9
E_g (164)											
$E_g(315)$	2.20	1.95	0.25	−28.1±2.5	−24.9	−3.2±2.6	0.89±0.08	32.30	2.36		9.5
$E_g(366.5)$	1.83	1.49	0.34	−27.2±1.0	−22.2	−5.0±1.1	0.81±0.04				

that γ^T is temperature independent and that, for the purpose of integration, one can take $\omega(T)\approx\omega(0)$. Since in our case γ^T depends on T, we employ Eq. (18a) to calculate $\Delta\omega_{\rm vol}$, using the slopes at 25 K and the known functions $\kappa(T)$ and $\beta(T)$ from Eqs. (4) and (9). The lower limit of integration is chosen at $T_0=0$ K. The results for $\Delta\omega_{\rm vol}(T)$ are shown in Fig. 9 by heavy solid lines.

Now that $\Delta\omega_{\rm total}(T)$ and $\Delta\omega_{\rm vol}(T)$ have been defined and calculated, we can proceed to the function $\Delta\omega_{\rm expl}(T)$ following Eq. (16). The results are shown by dots in Fig. 9. According to these results the phonon shift is totally due to the implicit term $\Delta\omega_{\rm vol}$ (volume expansion) for all phonons studied, except those at 79 and 146.5 $\rm cm^{-1}$. In other words, in most of the cases the total shift is equal to the volume-driven shift so that

$$\Delta\omega_{\rm total}-\Delta\omega_{\rm vol}=\Delta\omega_{\rm expl}=0\ . \tag{18d}$$

On the contrary, the phonons at 79 and 146.5 $\rm cm^{-1}$ exhibit large terms $\Delta\omega_{\rm expl}(T)$. Their description in terms of anharmonicity parameters will be discussed in Sec. VII. Lack of extensive data does not permit any statement to be made for the phonon at 230 $\rm cm^{-1}$.

VI. ISOTROPIC APPROXIMATION

The entire theoretical formulation developed in the preceding section was based on Eq. (13) for which we assumed validity of the isotropic approximation, that is, temperature independence of the ratio of lattice constants a_3/a_1. A more precise treatment of the thermodynamic relations would involve an explicit dependence of ω on a_1,a_3 rather than just on the volume of the unit cell. This distinction for uniaxial crystals was first pointed out by Peercy who showed that Eq. (13) is correct only for cubic materials and that for uniaxial crystals one should consider the following equation:[10,21]

$$\left[\frac{\partial\omega}{\partial T}\right]_P=(2\beta_1 a+\beta_3 b)+\left[\frac{\partial\omega}{\partial T}\right]_V\ . \tag{19}$$

The difference between Eqs. (13) and (19) lies in the volume-driven term. It is a matter of straightforward algebra to show that the two terms differ by

$$\begin{aligned}\alpha&\equiv-\beta\omega\gamma^T-(2\beta_1 a+\beta_3 b)\\&=\frac{2(\beta_1\kappa_3-\beta_3\kappa_1)}{\kappa}(a-b)\\&=\frac{2(\beta_1\kappa_3-\beta_3\kappa_1)}{\kappa S'}(\kappa_1 b'-\kappa_3 a')\ ,\end{aligned} \tag{20}$$

and that $\alpha\to0$ as the material changes from uniaxial to cubic (i.e., $\beta_1\to\beta_3\to\beta/3$, $\kappa_1\to\kappa_3\to\kappa/3$). The values for $-\beta\omega\gamma^T$, $2\beta_1 a+\beta_3 b$, their difference $\lvert\alpha\rvert$, and its percentage value are all listed in Table II for $T=300$ K. It becomes clear from the last column of Table II that the percentage deviation from the isotropic (cubic) approximation is less than 15% for all phonons studied. Although such percentages are not negligible, they nevertheless lead to variations of the various contributions well under their uncertainties due to experimental errors. It is interesting to note that in the case of rutile the deviations estimated by Peercy[10] were at most 10%. The conclusion of this

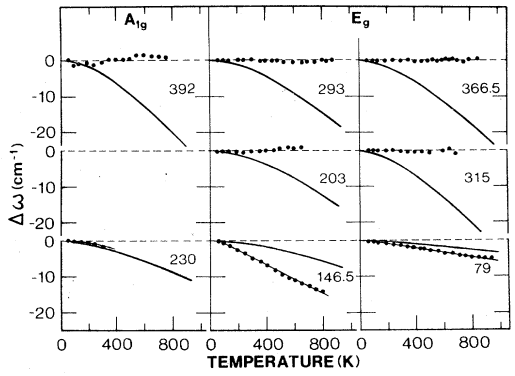

FIG. 9. Heavy solid lines $\Delta\omega_{\rm vol}$ from Eq. (18a) and Eqs. (4) and (9). Dots represent $\Delta\omega_{\rm expl}=\Delta\omega_{\rm total}-\Delta\omega_{\rm vol}$. The thin solid line represents the best fit of dots with Eq. (21). Dashed lines represent $\omega(0)$ from Fig. 2.

section is that, within the limits of the present experimental accuracy, the isotropic approximation, as expressed by Eq. (13), is well satisfied. It is reasonable to expect that repeating the above calculations at different temperatures will lead to the same conclusion.

VII. EXPLICIT CONTRIBUTIONS AND ANHARMONICITY

The explicit (or occupation number-driven) contributions to the frequency shifts discussed in Sec. V and shown by dots in Fig. 9, originate from third- and fourth-order anharmonic terms in the crystal Hamiltonian. Such terms are responsible for phonon decays to two and three new phonons, respectively, in such a way that the conservation of energy and momentum is satisfied. This problem has, in the past, been the subject of extensive theoretical[23] and experimental[16,20,24,25] work. The most commonly used model assumes decaying of the phonon with (harmonic) frequency ω_0 to two and three phonons of frequencies $\omega_0/2$ and $\omega_0/3$, respectively. The relevant expression for the explicit frequency shift is

$$\Delta\omega_{\text{expl}}=C(n_2+\tfrac{1}{2})-D[(n_3+\tfrac{1}{2})^2+\tfrac{1}{12}]+\frac{2D-3C}{6}\ , \tag{21}$$

where n_2 and n_3 are the phonon occupation numbers at $\omega_0/2$ and $\omega_0/3$, and C,D are non-negative constants. Because of the validity of the isotropic approximation (Sec. VI) we can assume that Eq. (2) is valid for LaF_3 too. The harmonic frequency ω_0 and the anharmonicity parameters C, D are then determined from the fitting of Eq. (21) to the data (dots) of Fig. 9.

An expression similar to Eq. (21) describes the T-dependent broadening of the phonon lines shown in Fig. 3,

$$\Gamma(T)=\Gamma_0+A(n_2+\tfrac{1}{2})+B[(n_3+\tfrac{1}{2})^2+\tfrac{1}{12}]\ , \tag{22}$$

where A,B are non-negative constants and Γ_0 is a term representing a residual broadening due to lattice imperfections. Again Γ_0,A,B will be defined from fitting of Eq. (22) to the data of Fig. 3.

The results of such fittings are included in Figs. 3 and 9, while the values of the constants $\omega_0,\Gamma_0,A,B,C,D$ are listed in Table III. Notice that according to Eqs. (16)–(18) and (21) we have $\omega(0)=\omega_0$. Only the phonons at 79 and 146.5 cm^{-1} were studied for their contributions $\Delta\omega_{\text{expl}}$, since these are the only ones which show such definite behavior.

From the values of Table III it is easily concluded that the main physical contribution to $\Delta\omega_{\text{expl}}$ arises from the three-phonon processes (two-phonon decaying), a behavior common to most of the materials studied thus far.[20,25,26] As far as the phonon linewidth is concerned, Table III suggests that although three-phonon processes appear to be responsible for most of the broadening, non-negligible contributions from four-phonon processes are also present. This is a situation similar to GaP according to the results of Bairamov *et al.*[16] Furthermore, LaF_3 is known to exhibit ionic conductivity due to the motion of fluorine ion vacancies.[27] In fact, at temperatures between 800 and 900 K it shows an anomalous increase in the fractional concentration of Schottky defects.[5] This is the region of topmost temperature values reached in the present work, since beyond these temperatures the material acquired a milky appearance and lost its optical quality. We tend to associate this transition to the large number of defects and to attribute some of the broadening in these high temperatures to a defect related mechanism. We feel that it is for the same reason that the data of Fig. 3 show no tendency for saturation at high temperatures, where at $T\to 0$ the usual behavior of bending to zero slope is observed.

TABLE III. Harmonic frequency $\omega_0=\omega(0)$ and anharmonicity parameters of Eqs. (21) and (22) determined from fitting to the data.

Symmetry D_{3d}^4	ω_0	Γ_0	A	B	C	D
A_{1g}	230	0	2.0	0.4	1.5[a]	0
	392	0	13.0	1.2	0	0
E_g	146.5	0	2.6	0.2	1.9	0
	203	0	2.3	0.8	0	0
	293	0	5.5	1.5	0	0
	299					
	79	0	0.3	0	0.4	0
	164					
	315	0	5.0	0.8	0	0
	366.5	5.5	3.0	2.5	0	0

[a]Tentative value based on available low-temperature data only (see Fig. 9).

VIII. DISCUSSION AND CONCLUSIONS

We have investigated the effects of hydrostatic pressure and temperature on most of the Raman-active phonons of LaF_3. The slopes $(d\omega/dP)_T$ were obtained from the variable pressure experiments at 25 and 300 K and were found independent of temperature. This fact combined with the T dependence of the phonon frequencies and of the elastic compliances lead to a measurable variation with temperature of the mode Grüneisen parameters γ^T. These are shown in Fig. 8 for some of the phonons.

The present values of γ^T shown in Table I vary between 1 and 2 (contrary to the values from uniaxial stress measurements which span a range from 0.15 to 2.24). This uniformity in the values of γ^T is characteristic of a large variety of materials such as tetrahedrally bonded semiconductors, simple ionic solids, and molecular crystals[22] (external modes). On the contrary, internal modes of molecular crystals exhibit Grüneisen parameters that follow a scaling law of the type $\gamma^T\sim\omega^{-2}$. No such correlation could be established in the present values, and this is consistent with the fact that the LaF_3 is an ionic crystal[27] with phonons which have no physical resemblance to internal modes. The prevailing ionic character of LaF_3 has also been inferred independently from the analysis of the dispersion of its index of refraction.[9] Finally, we notice with interest the general trend of the slopes $(d\omega/dP)_T$ to increase with ω, a behavior opposite to that of molecu-

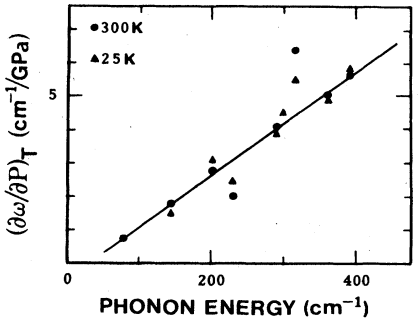

FIG. 10. Pressure slopes as a function of phonon frequency at $T=25$ K and 300 K. The solid line fits the 25 K data.

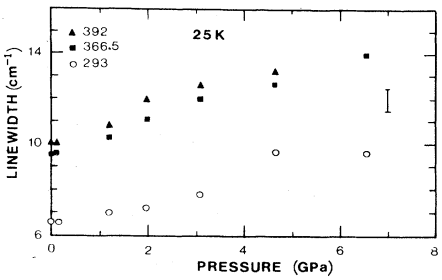

FIG. 11. Phonon linewidths as a function of pressure at $T=25$ K for three of the long-wavelength optical phonons studied.

lar crystals.[21] Figure 10 shows the situation. We use the 25 K data of Fig. 10 with an approximate linear fit to deduce a value for the slope $(\partial\omega/\partial P)_T$ of the phonon at 79 cm^{-1}, which was not measured at 25 K. The value obtained in this way is (0.70 ± 0.03) cm^{-1}/GPa and is nearly equal to the value 0.83 ± 0.04 observed for the same slope at 300 K. This is in accord with the present general situation, whereupon the slopes $(\partial\omega/\partial P)_T$ are independent of T.

A final comment concerning the pressure measurements is the dependence of the phonon linewidth Γ on P. Such dependence was in fact observed. The cases of modes where the experimental accuracy allowed quantitative measurements of $\Gamma(P)$ are shown in Fig. 11. In all three cases the trend for Γ is to increase with P almost linearly with a slope between 0.4 and 0.7 cm^{-1}/GPa. Similar behavior was recently observed in GaAs where, under compression with a uniaxial stress along [111], the piezoreflectance spectra showed an increase of the $T0$ phonon linewidth at a rate of 0.3 cm^{-1}/GPa.[28] Such variations are attributed to shifting of the phonon frequencies relative to the spectrum of the phonon density of states. They are rather small to be taken into consideration when dealing with the much larger changes of Γ due to T. They nevertheless pose an interesting problem for an independent investigation.

The main conclusion in connection with the observed shifts $\Delta\omega_{\text{total}}(T)$ is that in most of the cases such shifts are almost exclusively accounted for by volume expansion. This is clearly evident in Fig. 9, where for most of the phonons the value of $\Delta\omega_{\text{expl}}$ is zero. It is interesting that all these phonons involve motions of the fluorine atoms.[3] The phonons at 79 and 146.5 cm^{-1}, on the other hand, exhibit rather strong anharmonic behavior (solid lines in Fig. 9). Contrary to the previous cases, these modes involve motions of the lanthanum atoms.[3] An alternative way of visualizing the relative contributions of volume and anharmonicity is to use the implicit fraction $\eta=\gamma^T/\gamma^P$, that is, the ratio of the volume contribution to the observed total effect. For the phonons with no anharmonic contributions (fluorine motion) Table II gives $\eta\approx1$. For the phonons at 79 and 146.5 cm^{-1} (lanthanum motion, large anharmonicity) Table II gives $\eta<0.5$. According to a general classification scheme[22] the former values of η characterize ionic crystals or external modes from molecular crystals, while the latter values of η correspond to covalent crystals or internal modes from molecular crystals. In our case it might be concluded that, while the fluorine atoms which participate in most of the phonons are subject to ionic bonding, the lanthanum atoms involved in the few phonons mentioned above are subject to covalent bonding. No eigenvector analysis of the LaF_3 modes is available to our knowledge. Therefore, it is not possible to further elaborate on this matter.

ACKNOWLEDGMENTS

We wish to thank Professor F. Cerdeira for making available to us the LaF_3 samples used in this work. One of us (G. A. K.) acknowledges valuable discussions with Dr. H. D. Hochheimer and technical assistance of Mr. W. Dieterich of the Max-Planck Institut, Stuttgart, concerning the 25 K measurements under hydrostatic pressure. This work was supported by the Ministry of Research and Technology, Greece.

[1]J. B. Mooney, Infrared Phys. **6**, 153 (1966).
[2]W. S. Heaps, L. R. Ellias, and W. M. Yen, Phys. Rev. B **13**, 94 (1976).
[3]R. P. Bauman and S. P. S. Porto, Phys. Rev. **161**, 842 (1967).
[4]F. Cerdeira, V. Lemos, and R. S. Katiyar, Phys. Rev. B **19**, 5413 (1979).
[5]A. Sher, R. Solomon, K. Lee, and M. W. Müller, Phys. Rev. **144**, 593 (1966).
[6]J. R. Igel, M. C. Wintersgill, J. F. Fontanella, A. V. Chadwick, C. G. Andeen, and V. E. Bean, J. Phys. C **15**, 7215 (1982).
[7]D. A. Jones and W. A. Shand, J. Cryst. Growth. **2**, 361 (1968); L. G. Van Uiter, H. M. O'Bryan, H. J. Guggenheim, R. L. Barns, and G. Zydzik, Mater. Res. Bull. **12**, 307 (1977).
[8]R. Laiho, M. Lakkisto, and T. Levola, Philos. Mag A **47**, 235 (1983).
[9]R. Laiho and M. Lakkisto, Philos Mag. B **48**, 203 (1983).
[10]P. S. Peercy, Phys. Rev. B **8**, 6018 (1973).
[11]A. K. Arora and V. Umadevi, Appl. Spectrosc. **36**, 424 (1982).
[12]K. R. Hirsch and W. B. Holzapfel, Rev. Sci. Instrum. **52**, 52 (1981); G. A. Kourouklis, A. K. Sood, H. D. Hochheimer, and A. Jayaraman, Phys. Rev. B **31**, 8332 (1985).
[13]J. D. Barnett, S. Block, and G. J. Piermarini, Rev. Sci. Instrum. **44**, 1 (1973).
[14]F. D. Murnaghan, Proc. Natl. Acad. Sci. U.S.A. **30**, 244

(1944).
[15]J. F. Nye, *Physical Properties of Crystals* (Clarendon, Oxford, 1964), p. 146.
[16]B. Bairamov, Yu. E. Kitaev, V. K. Negoduiko, and Z. M. Khashkhozhev, Fiz. Tverd. Tela (Leningrad) **16**, 2036 (1974) [Sov. Phys. Solid State **16**, 1323 (1975)].
[17]*Handbook of Mathematical Functions,* edited by M. Abramowitz and I. Stegan (Dover, New York, 1972), p. 998.
[18]E. L. Slaggie, Phys. Rev. B **2**, 2230 (1970); R. J. Elliott, W. Hayes, W. G. Kleppmann, A. J. Rushworth, and J. F. Ryan, Proc. R. Soc. London, Ser. A **360**, 317 (1978).
[19]V. V. Baptizmanskii, I. I. Novak, and Yu. F. Titovets, Sov. Phys. Solid State **21**, 1915 (1979).
[20]V. G. Khamdamov, V. I. Vettegren, and I. I. Novak, Fiz. Tverd. Tela (Leningrad) **22**, 3242 (1980) [Sov. Phys. Solid State **22**, 1896 (1980)].
[21]F. Cerdeira, F. E. A. Melo, and V. Lemos, Phys. Rev. B **27**, 7716 (1983).
[22]B. A. Weinstein and R. Zallen, in *Topics in Applied Physics,* edited by M. Cardona and G. Güntherodt (Springer, Heidelberg, 1984), Vol. 54, p. 463.
[23]R. F. Wallis, I. P. Ipatova, and A. A. Maradudin, Fiz. Tverd. Tela (Leningrad) **8**, 1064 (1966) [Sov. Phys. Solid State **8**, 850 (1966)]; I. P. Ipatova, A. A. Maradudin, and R. F. Wallis, Phys. Rev. **155**, 882 (1967).
[24]M. Balkanski, R. F. Wallis, and E. Haro, Phys. Rev. B **28**, 1928 (1983).
[25]E. Liarokapis and E. Anastassakis, Phys. Rev. B **30**, 2270 (1984); and also in *Raman Spectroscopy, Proceedings of the IXth International Conference on Raman Spectroscopy* (The Chemical Society of Japan, Tokyo, 1984), p. 400.
[26]B. Jusserand and J. Sapriel, Phys. Rev. B **24**, 7194 (1981).
[27]R. Solomon, A. Sher, and M. W. Müller, J. Appl. Phys. **37**, 324 (1966).
[28]M. Hünermann, J. Saalmüller, W. Richter, and E. Anastassakis (unpublished).
[29]M. Dahl and G. Schaack, J. Lumin. **31**, 84 (1984).